Supplementary

1 Hardware System

The 3D tracking system is primarily composed of two subsystems: the magnetic field generating subsystem and the magnetic field perceiving subsystem (Fig. 1). The field generating subsystem consists of multiple transmitter coils, each driven by an H-bridge circuit capable of producing controlled alternating magnetic fields (Fig. 2). These coils are typically distributed spatially in the environment or on objects of interest. Each H-bridge operates as a switching amplifier that converts digital control signals into bidirectional current excitation through the transmitter coils. By selectively modulating each coil at a distinct time slot, the system creates a spatially varying and temporally separable magnetic field distribution. This is illustrated in the central of Fig. 1, which visualizes the magnetic field intensities as a spatially smooth and centered gradient, ideal for multilateration-based localization. The field perceiving subsystem begins with a passive receiver coil that detects the magnetic field strength at its location. The induced signal is then passed to a two-stage analog signal processing circuit. The first stage includes a linear amplifier and frequency selection filter, which isolates the frequency band of interest corresponding to a specific transmitter. This stage enhances signal quality and suppresses out-of-band noise. The filtered analog signal is then routed to a logarithmic amplifier, which compresses the signal dynamic range and facilitates robust amplitude tracking across a wide range of field intensities. This processed analog voltage is finally digitized by an ADC for further computational processing (Fig. 3).

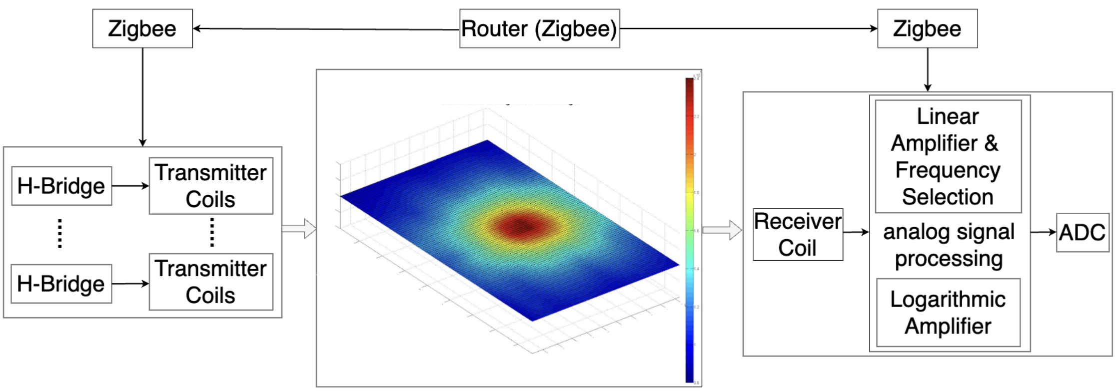

Fig. 1: The hardware system diagram

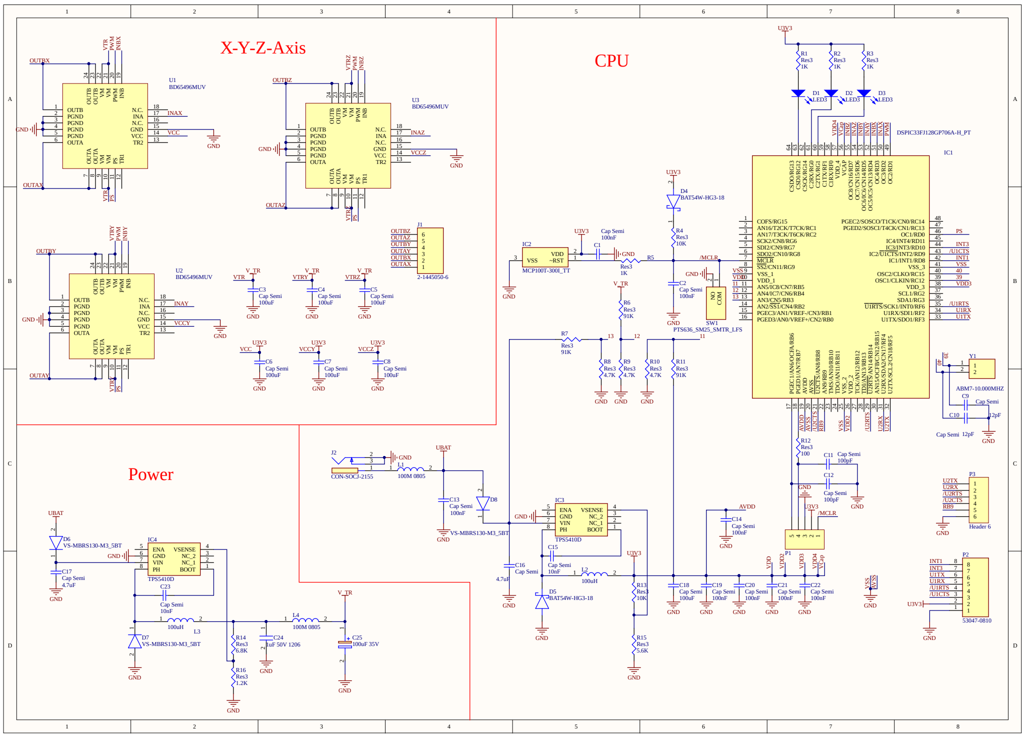

Fig. 2: The transmitter system schematic

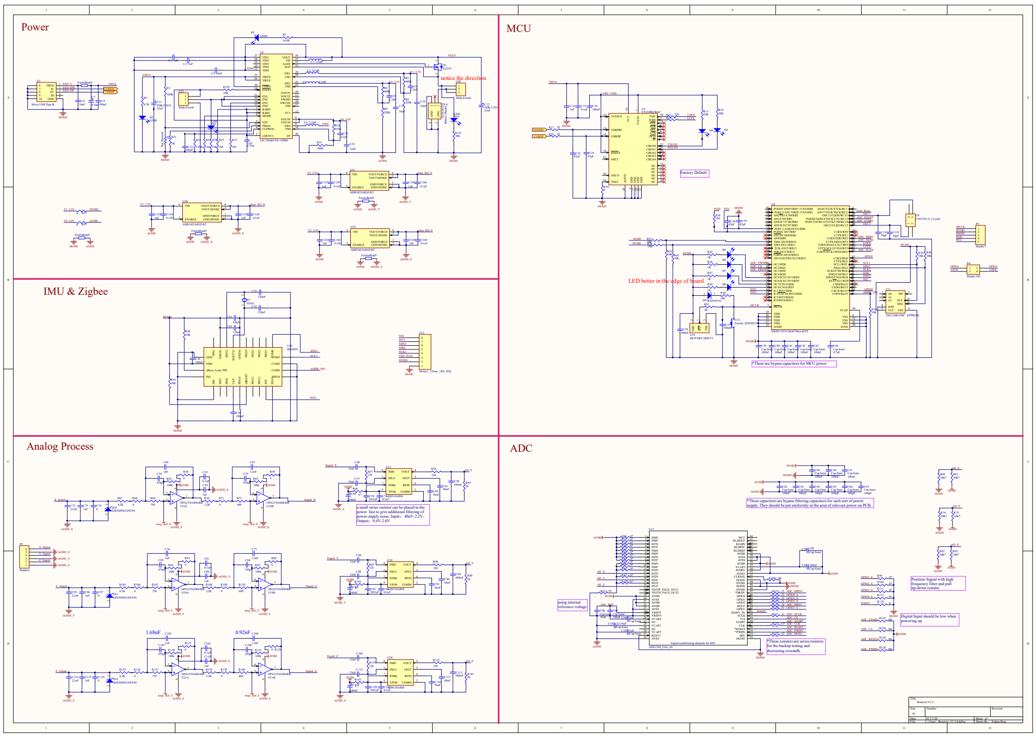

Fig. 3: The receiver system schematic

1.1 Transmitter

The H-Bridge is used to drive the resonance circuit in three axes with the square wave from the dsPIC33FJ128GP706. A resonance circuit generates a magnetic field, with the amplitude of the induced voltage reaching its maximum. The peak value of the induced voltage is proportional to the amplitude of the driving current.

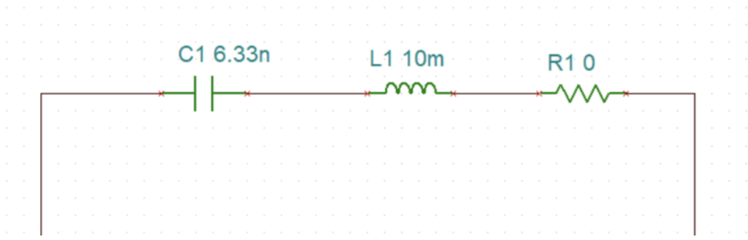

Fig. 4: Resonant Circuit at Transmitter Side

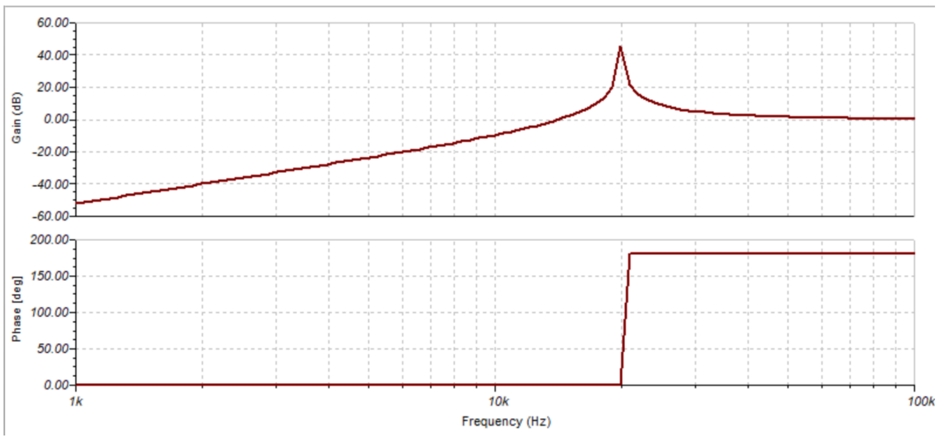

Fig. 5: Transfer Characteristic

The transfer characteristic of the current in this resonance circuit is shown in Fig. 5. As shown, to get a maximum peak value of the current in the coils, the resonant frequency, which needs to be tuned throught the LC tank circuit, should equal the frequency of the current.

In engineering, the Q factor is a dimensionless parameter that describes how under-damped a resonator is and characterizes its bandwidth relative to its center frequency. Suppose f_0 is the resonance frequency, with $I(w) = I_m$, f_1 and f_2 is the cut-off frequency, with $I(w) = I_m/1.404$.

$$Q = \frac{f_0}{f_2 - f_1} \tag{1}$$

This indicates that getting a higher Q factor benefits the signal-to-noise ratio and precise resonance.

After debugging the software and adjusting the transmitter coils, the voltage amplitude in the coil reaches its maximum value. The expected parameters are listed in Tables 1.

Table 1: Practical oscillating result among six transmitter coils under excitation of 5V/20Khz

Transmitters	Pk-Pk (V)	Frequency (KHz)	Duty (%)
T1	105.25	20.02	49.97
T2	108.34	19.97	50.00
T3	102.96	20.04	50.03
T4	108.78	20.01	49.99
T5	105.45	19.98	49.99
T6	100.29	20.02	50.01

∗Data were measured by a Tektronix TDS 2002 oscilloscope. Small deviations in frequency and duty were caused mainly by the component tolerance.

1.2 Receiver

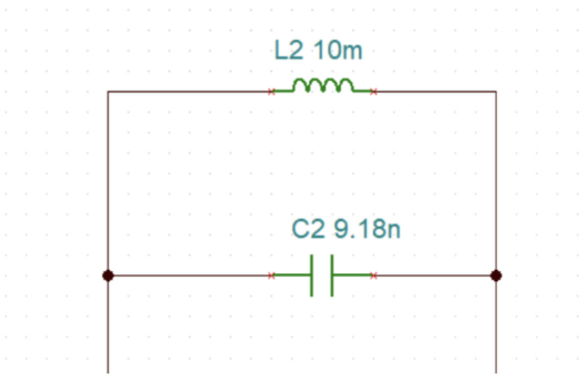

Fig. 6: Resonant Circuit at Receiver Side

Fig. 6 shows the LC parallel circuit with a resonant frequency of 20 kHz. In an ideal series RLC circuit, as in a tuned radio frequency receiver, the Q factor equals:

$$Q = \frac{1}{R}\sqrt{\frac{L}{C}} = \frac{\omega_0 L}{R} \tag{2}$$

Where R, L, and C are the resistance, inductance, and capacitance of the tuned circuit, respectively. The larger the series resistance, the lower the circuit Q. For a parallel RLC circuit, the Q factor is the inverse of the series case:

$$Q = R\sqrt{\frac{C}{L}} = \frac{R}{\omega_0 L} = \omega_0 RC \tag{3}$$

In a parallel LC circuit, the main loss is the resistance of the inductor R_L, in series with the inductance L. This is a common circumstance for resonators, where limiting the resistance of the inductor to improve Q and narrow the bandwidth is the desired result. The strength of a signal in space is inversely proportional to the cube of the distance from the signal source to the measured position. To achieve a wide detection distance, a receiver coil with a high Q quality is desired.

1.3 Analog Signal Processing

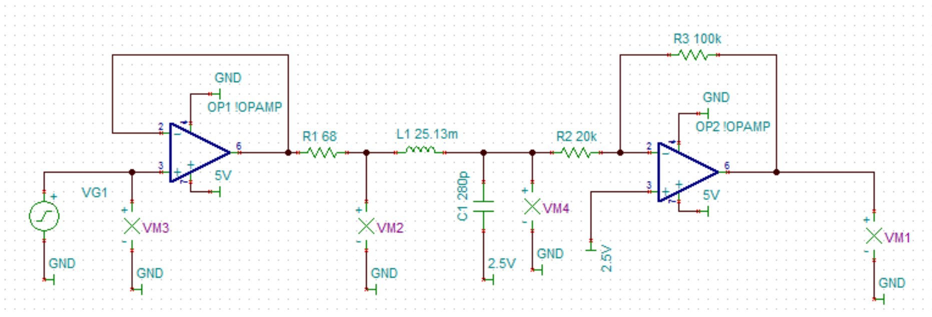

Fig. 7: Butterworth Filter and Amplifier

As Fig. 7 depicts, after the receive coil induces the voltage signal, a two-level amplifier and a logarithmic amplifier are used to amplify the signal. OPA378 is a low-noise, zero-drift operational amplifier from TI with the Gain-Bandwidth Product up to 900KHz. The combination of low input voltage noise, high gain bandwidth, and low power enables it to achieve optimum performance for high-precision applications. The first amplifier is used as a voltage buffer to provide a low output impedance, and the second amplifier enlarges the signal by five times with negative feedback. It is worth noting that, as a low-pass filter, C1 and L1 in the circuit also have an amplified action on the voltage signal. This part's main purpose is to amplify the induced voltage signal. Another significant function is to filter the signal so that the signal entering the log amp is stable and as clear as a single-frequency signal. The essential purpose of the logarithmic amp is not to amplify (though amplification is needed internally) but to compress the signal with a wide dynamic range from the preamp to its decibel equivalent. AD8310 from Analog Devices, with a large dynamic range and fast response time, is used as a received signal strength indicator, converting the voltage from signal level into decibels. The logarithmic amplifier acts both as a linear and a logarithmic amplifier while working. When the input signal is weak, it is a linear amplifier with a larger gain; otherwise, it becomes a logarithmic amplifier with a decreasing gain when the input signal increases.

1.4 Magnetic Field Triggering and Signal Acquisition Protocol

Figure 8 depicts the embedded scheduling protocol implemented in the transmitter–receiver firmware and illustrates a representative example of the acquired magnetic field signal. A central router coordinates the activation of individual transmitter coils by broadcasting their unique identifiers to each Zigbee-enabled unit every 50 ms. Upon receiving this command, the corresponding transmitter coil initiates a 20 kHz oscillation, driven by an on-board H-bridge and controlled via a pulse-width modulated (PWM) waveform generated by the microcontroller. The excitation period for each transmitter is configured to last 40 ms, allowing sufficient time for magnetic field stabilization and energy buildup.

On the receiver side, the microcontroller listens for the broadcasted activation signal and initiates a delayed acquisition sequence. Specifically, the onboard analog-to-digital converter (ADC) begins

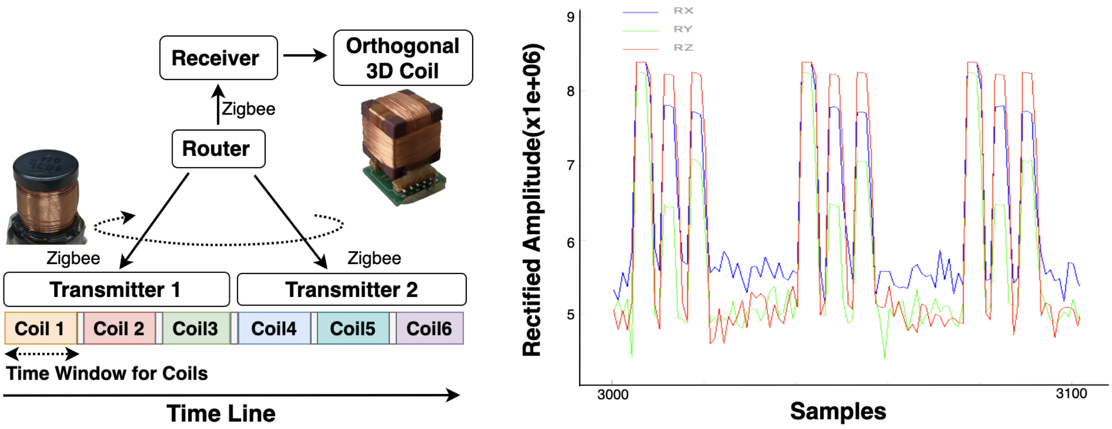

Fig. 8: Firmware protocol of the hardware system

sampling after a 5 ms wait period to allow transient oscillations to settle. It then samples the induced voltage signal for a duration of 30 ms at a resolution of 1 kHz. This schedule ensures low-noise acquisition while minimizing overlap between consecutive transmitter activations.

The captured signal is transmitted in real time to a nearby processing device either via a TTL-to-USB serial connection or over a wireless Bluetooth link, depending on deployment needs. A representative time-series signal example is shown, depicting the sequentially triggered responses from three transmitter coils (out of a six-coil setup) as recorded by the orthogonal tri-axis receiver. These signal traces capture the temporal and spatial characteristics of magnetic field strength across different axes, forming the basis for downstream tracking or classification tasks.

2 Justification of Crosstalk Tolerance

In the tri-axis receiver coil, measured crosstalk between orthogonal windings was maintained below 22%. This refers to the maximum induced voltage observed in a non-aligned coil axis relative to the primary axis when excited by a single transmitter. While nonzero, this level of crosstalk does not significantly degrade the accuracy of magnetic field-based positioning due to the following physical and computational factors.

First, consider the induced voltage components across three orthogonal axes: $V_1 = 1.0$ (normalized primary signal), $V_2 = V_3 = 0.22$ (crosstalk components). The magnitude of the composite magnetic field vector is:

$$B_{\text{eff}} = \sqrt{V_1^2 + V_2^2 + V_3^2} = \sqrt{1.0^2 + 0.22^2 + 0.22^2} \approx 1.047 \tag{4}$$

This yields a relative deviation from the ideal (crosstalk-free) magnitude of only:

$$\frac{B_{\text{eff}} - B_{\text{ideal}}}{B_{\text{ideal}}} = \frac{1.047 - 1.0}{1.0} = 4.7\% \tag{5}$$

Second, due to the near-field nature of magnetic induction, the field strength decays with the cube of distance ($B \propto 1/r^3$). Thus, any spatial offset between coil windings further reduces the effective magnetic influence of crosstalk components. For example, a 10 cm offset relative to a 20 cm primary distance results in:

$$\left(\frac{r}{r+\Delta r}\right)^3 = \left(\frac{20}{30}\right)^3 \approx 0.296 \tag{6}$$

This steep decay mitigates the contribution of non-primary components in spatially distributed sensing setups.

Third, the crosstalk is deterministic and consistent across repeated measurements. Therefore, data-driven models, such as our physics-informed deep learning architecture, can learn to implicitly correct for such systematic interference.

In practice, we observe that the 22% inter-axis crosstalk does not obviously impair the vector directionality required for reliable 3D inference. This is confirmed empirically by the sub-3.0 centimeter accuracy achieved in coordinate regression tasks.

3 Voltage Ratio VS. Frequency Ratio For Frequency Selection

In an LRC series circuit, assuming that the voltage source is $\dot{U}$, angular frequency is ω, the impedance of every discrete component is:

$$Z_R = R, \quad Z_L = j\omega L, \quad Z_C = \frac{1}{j\omega C} \tag{7}$$

The total impedance of this series circuit is

$$Z = R + j\left(\omega L - \frac{1}{\omega C}\right) \tag{8}$$

The Current in the series circuit is

$$\dot{i} = \frac{\dot{U}}{Z} = \frac{\dot{U}}{R + j\left(\omega L - \frac{1}{\omega C}\right)} \tag{9}$$

The RMS of current is

$$I = \frac{U}{|Z|} = \frac{U}{\sqrt{R^2 + \left(\omega L - \frac{1}{\omega C}\right)^2}} \tag{10}$$

The Phase Difference between the voltage and current is

$$\varphi = \arctan\left(\frac{\omega L - \frac{1}{\omega C}}{R}\right) \tag{11}$$

Those parameters are all functions of ω, as shown in Fig. 9:

We can easily calculate the RMS of voltage for every discrete component based on current:

$$U_R = RI = \frac{R}{\sqrt{R^2 + \left(\omega L - \frac{1}{\omega C}\right)^2}} U \tag{12}$$

$$U_L = \omega L I = \frac{\omega L}{\sqrt{R^2 + \left(\omega L - \frac{1}{\omega C}\right)^2}} U \tag{13}$$

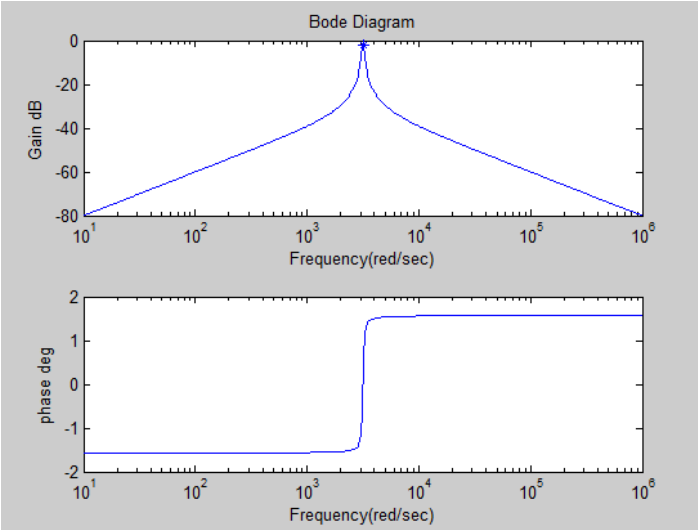

Fig. 9: Current in the series circuit vs. frequency

$$U_C = \frac{I}{\omega C} = \frac{1}{\omega C\sqrt{R^2 + \left(\omega L - \frac{1}{\omega C}\right)^2}} U \tag{14}$$

These three formulas express the Magnitude-Frequency characteristic of the component R, L, and C. When $\frac{1}{\omega C} = \omega L$, $\varphi = 0$, current and voltage are in phase, the circuit is in series resonant. The resonant angular frequency is

$$\omega_0 = \frac{1}{\sqrt{LC}} \tag{15}$$

From formulas 12, 13, 14, when the frequency reaches the resonant frequency, I and U_R reach their maximum, but the maximum of U_L and U_C do not appear at the point of resonant frequency. Still, they can be easily calculated from formulas 13 and 14, and the resonant frequency of the corresponding maximum U_{LM} and U_{CM} are:

$$\omega_L = \sqrt{\frac{2}{2LC - R^2C^2}} \tag{16}$$

$$\omega_C = \sqrt{\frac{1}{LC} - \frac{R^2}{2L^2}} \tag{17}$$

For a resonant circuit, the quality factor is:

$$Q = \frac{\omega_0 L}{R} = \frac{1}{\omega_0 CR} \tag{18}$$

Incorporating formulas 16, 17, 18, , we can get:

$$\omega_L = \frac{1}{\sqrt{1 - \frac{1}{2Q^2}}}\omega_0 \tag{19}$$

$$\omega_C = \sqrt{1 - \frac{1}{2Q^2}}\,\omega_0 \tag{20}$$

When $Q > \frac{1}{\sqrt{2}}$, we get the corresponding maximum value:

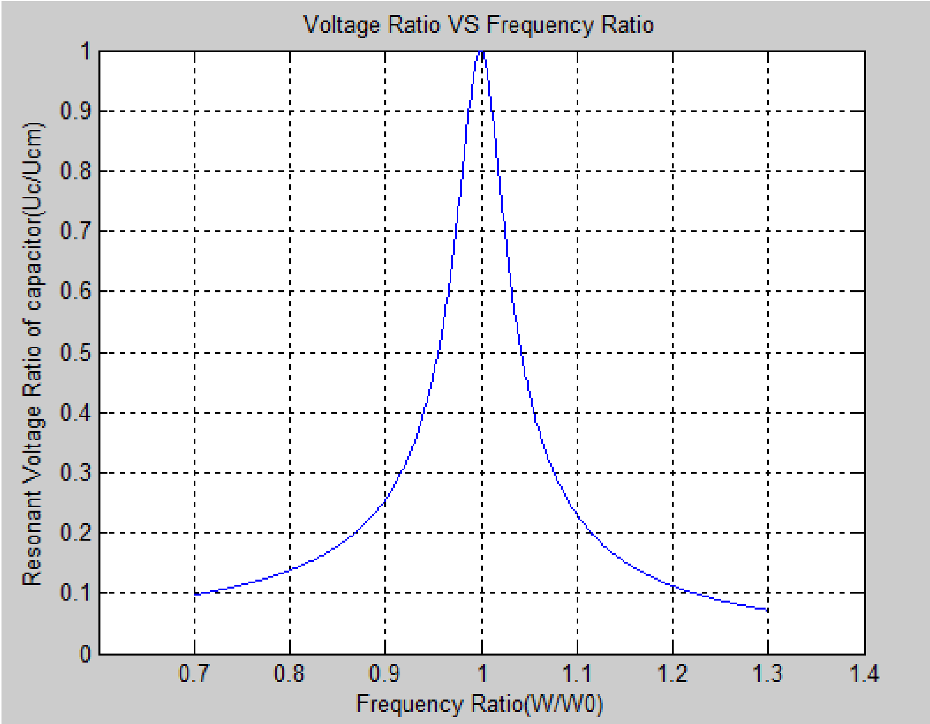

Fig. 10: Voltage Ratio VS Frequency Ratio(RLC Circuit)

$$U_{LM} = U_{CM} = \frac{QU_M}{\sqrt{1 - \frac{1}{4Q^2}}} \tag{21}$$

Here U_M is the resistance voltage when the angular frequency is the same with the resonant frequency.

Assuming that we need to calculate a frequency ω so that the voltage of the resonant capacitor is:

$$U_C = k_1 U_{CM} \tag{22}$$

$$U_L = k_2 U_{LM} \tag{23}$$

Where k is a factor that we give according to the demand of the application. With formulas 14, 18, 21, we can calculate the factor k_1:

$$
\begin{aligned}
k_1 = \frac{U_C}{U_{CM}} &= \frac{\sqrt{4Q^2-1}}{2Q^2\omega C\sqrt{R^2+\left(\omega L-\frac{1}{\omega C}\right)^2}} \\
&= \frac{\sqrt{4Q^2-1}}{2Q^2R\omega C\sqrt{1+\left(\frac{\omega L-\frac{1}{\omega C}}{R}\right)^2}} \\
&= \frac{\sqrt{4Q^2-1}}{2Q^2\cdot\frac{\omega RC\omega_0}{\omega_0}\sqrt{1+\left(\frac{\omega\omega_0 L}{\omega_0 R}-\frac{\omega_0}{\omega_0 CR}\right)^2}} \\
&= \frac{\sqrt{4Q^2-1}}{2Q^2\cdot\frac{\omega}{\omega_0}\cdot\frac{1}{Q}\sqrt{1+\left(\frac{\omega}{\omega_0}\cdot Q-\frac{\omega_0}{\omega}\cdot Q\right)^2}} \\
&= \frac{\sqrt{4Q^2-1}}{2Q\cdot\frac{\omega}{\omega_0}\sqrt{1+\left(\frac{\omega}{\omega_0}-\frac{\omega_0}{\omega}\right)^2Q^2}}
\end{aligned} \tag{24}
$$

Assuming that $\frac{\omega}{\omega_0} = m$, then:

$$
k_1 = \frac{\sqrt{4Q^2-1}}{2Qm\sqrt{1+\left(m-\frac{1}{m}\right)^2Q^2}} \tag{25}
$$

In the same way, we can calculate the factor k_2:

$$
k_2 = \frac{\sqrt{4Q^2-1}}{2Qm\sqrt{1+\left(m-\frac{1}{m}\right)^2Q^2}} \tag{26}
$$

Q is the quality characteristic of a resonant circuit, which is only related to the parameter of the resonant circuit. For example, the variation of frequency has no effect on the value of quality characteristic. That is to say, formulas 25, 26 are functions of single variable.

Fig. 10 shows the relationship between voltage ratio and frequency ratio of a discrete component in a series resonant circuit(Q=20). A negligible tiny shift of the frequency ω from ω_0 can be observed when reaching the highest voltage on the capacitor (same case for inductor). Formula 24 can provide a more precise calculation.

4 Robustness to Metallic Object Interference

To evaluate the practical deployment viability of our magnetic field-based 3D tracking system, we conducted robustness assessments focused on the system's sensitivity to nearby metallic objects. This evaluation is essential for ensuring reliable operation in real-world contexts where users may handle or interact with metal-based tools, electronic devices, or infrastructure, such as in industrial assembly, smart manufacturing, or augmented reality workspaces.

In a controlled experimental setup, a metallic object, specifically, a brushed stepper motor with conductive casing and internal windings, was brought progressively closer to the receiver coil while recording the induced magnetic field signal. The metric used was the variation in rectified amplitude, which reflects the net magnetic field magnitude as sensed by the tri-axis receiver.

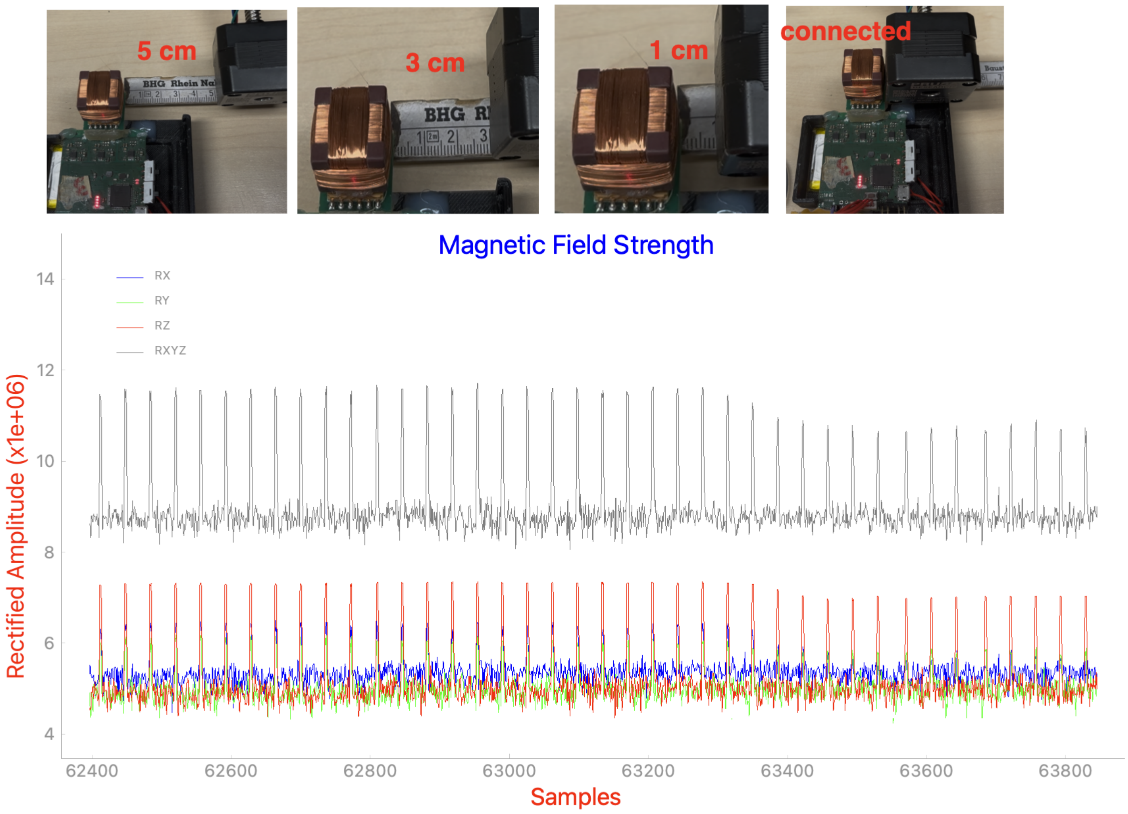

Fig. 11: Perceived strength signal variation against closing metallic object

The results (Fig. 11) reveal that the presence of metallic materials introduces only minor perturbations to the sensed field when the object is more than 1 cm away from the receiver. Notably, a measurable shift in signal strength is observed only when the metallic item approaches within sub-centimeter proximity, where mutual inductive effects and eddy current shielding begin to influence local field dynamics. At separations of 2 cm and beyond—which is typical in wearable applications such as wrist or finger-mounted tracking—the deviation in signal amplitude remains within acceptable margins for reliable trajectory estimation. The same conclusion also applied for the robustness test at the transmitter side.

These findings confirm that the system is inherently resilient to moderate environmental perturbations caused by passive metallic interference. Unlike high-frequency RF systems that are susceptible to multipath and conductive scattering, the low-frequency, quasi-static nature of magnetic induction exhibits significantly reduced sensitivity to common metal objects. In practice, when the receiver coil is positioned on the dorsum of the hand or fingertip, accurate motion tracking is preserved even during interactions with metallic surfaces or instruments (as demonstrated by the 3D tracking experiment of ”Sorting Hardware Tools”).

This dual-sided robustness extends the applicability of the proposed system to a wide range of real-world tasks involving tools, appliances, and embedded environments, reinforcing its practicality for deployment in manufacturing lines, clinical instruments, and everyday human–object interaction scenarios.

5 Effect of Transmitter Coil Number on Tracking Accuracy

Table 2: Effect of transmitter coil number on 3D tracking accuracy.

Number of Active Transmitter Coils	ATE (cm)
6 (A, B, C, D, E, F)	2.5
5 (A, B, D, E, F)	2.7
4 (A, B, D, E)	3.8
3 (A, B, D)	5.9
2 (A, D)	8.5
1 (A)	>10 (unreliable)

(Coil ID) Top left to right: A, B, C; Bottom left to right: D, E, F.

To evaluate the influence of transmitter coil count on the accuracy of near-range magnetic field tracking, we conducted a controlled ablation study using our tabletop experimental setup(the entertainment activity with Lego Bricks experiment). The environment was initially configured with six spatially distributed transmitter coils, enabling full spatial coverage and maximal signal diversity. We then systematically reduced the number of active transmitters to assess how signal sparsity affects coordinate estimation performance.

Tracking accuracy was quantified using the absolute trajectory error (ATE) metric under different coil activation configurations. As anticipated, reducing the number of transmitters led to a progressive decline in accuracy, reflecting the system's reliance on multilateration from multiple spatially separated sources. Nonetheless, with only four active coils, the degradation in accuracy was modest, with an average increase in ATE of just 1.3 cm, compared to the six-coil baseline. This suggests that the system retains robustness under moderate hardware reduction, owing to its ability to infer spatial structure from partial field information.

When the number of transmitters was reduced to two, tracking remained viable, with an average ATE of approximately 6.5 cm. However, this level of performance may be insufficient for applications demanding high-resolution hand or finger tracking. In contrast, with only a single transmitter, spatial ambiguity increased markedly, resulting in mean errors exceeding 10 cm, thereby rendering accurate localization impractical under such minimal configurations.

These results demonstrate that magnetic field-based positioning systems benefit substantially from signal diversity and spatial redundancy. Importantly, the system architecture supports seamless scalability: additional coils can be incorporated with minimal hardware reconfiguration or computational burden. Each added transmitter expands the effective coverage area and enhances geometric constraints for coordinate inference. Moreover, the low inter-coil interference and efficient signal scheduling ensure that increased coil count does not compromise real-time performance. This makes the system well-suited for adaptation to larger-scale or multi-user interactive environments where higher precision and broader spatial coverage are essential.